

Density Fluctuations in the Solar Wind Based on Type III Radio Bursts Observed by Parker Solar Probe

VRATISLAV KRUPAR,^{1,2,3} ADAM SZABO,² MILAN MAKSIMOVIC,⁴ OKSANA KRUPAROVA,³ EDUARD P. KONTAR,⁵
LAURA A. BALMACEA,^{2,6} XAVIER BONNIN,⁴ STUART D. BALE,^{7,8,9,10} MARC PULUPA,⁸ DAVID M. MALASPINA,¹¹
JOHN W. BONNELL,⁸ PETER R. HARVEY,⁸ KEITH GOETZ,¹² THIERRY DUDOK DE WIT,¹³ ROBERT J. MACDOWALL,¹⁴
JUSTIN C. KASPER,^{15,16} ANTHONY W. CASE,¹⁶ KELLY E. KORRECK,¹⁶ DAVIN E. LARSON,⁸ ROBERTO LIVI,⁸
MICHAEL L. STEVENS,¹⁶ PHYLLIS L. WHITTLESEY,⁸ AND ALEXANDER M. HEGEDUS¹⁵

¹*Universities Space Research Association, Columbia, MD 21046, USA*

²*Heliospheric Physics Laboratory, Heliophysics Division, NASA Goddard Space Flight Center, Greenbelt, MD 20771, USA*

³*Department of Space Physics, Institute of Atmospheric Physics of the Czech Academy of Sciences, Prague 14131, Czech Republic*

⁴*LESIA, Observatoire de Paris, Université PSL, CNRS, Sorbonne Université, Université de Paris, 92195 Meudon, France*

⁵*School of Physics and Astronomy, University of Glasgow, Glasgow G12 8QQ, UK*

⁶*George Mason University, Arlington, VA 22030, USA*

⁷*Physics Department, University of California, Berkeley, CA 94720-7300, USA*

⁸*Space Sciences Laboratory, University of California, Berkeley, CA 94720-7450, USA*

⁹*The Blackett Laboratory, Imperial College London, London, SW7 2AZ, UK*

¹⁰*School of Physics and Astronomy, Queen Mary University of London, London E1 4NS, UK*

¹¹*Laboratory for Atmospheric and Space Physics, University of Colorado, Boulder, CO 80303, USA*

¹²*School of Physics and Astronomy, University of Minnesota, Minneapolis, MN 55455, USA*

¹³*LPC2E, CNRS and University of Orléans, Orléans, France*

¹⁴*Solar System Exploration Division, NASA Goddard Space Flight Center, Greenbelt, MD 20771, USA*

¹⁵*Climate and Space Sciences and Engineering, University of Michigan, Ann Arbor, MI 48109, USA*

¹⁶*Smithsonian Astrophysical Observatory, Cambridge, MA 02138, USA*

(Received September 13, 2019; Accepted December 22, 2019)

Submitted to ApJS

ABSTRACT

Radio waves are strongly scattered in the solar wind, so that their apparent sources seem to be considerably larger and shifted than the actual ones. Since the scattering depends on the spectrum of density turbulence, better understanding of the radio wave propagation provides indirect information on the relative density fluctuations $\epsilon = \langle \delta n \rangle / \langle n \rangle$ at the effective turbulence scale length. Here, we have analyzed 30 type III bursts detected by Parker Solar Probe (PSP). For the first time, we have retrieved type III burst decay times τ_d between 1 MHz and 10 MHz thanks to an unparalleled temporal resolution of PSP. We observed a significant deviation in a power-law slope for frequencies above 1 MHz when compared to previous measurements below 1 MHz by the twin-spacecraft Solar TErrestrial RElations Observatory (*STEREO*) mission. We note that altitudes of radio bursts generated at 1 MHz roughly coincide with an expected location of the Alfvén point, where the solar wind becomes super-Alfvénic. By comparing PSP observations and Monte Carlo simulations we predict relative density fluctuations ϵ at the effective turbulence scale length at radial distances between $2.5 R_\odot$ and $14 R_\odot$ to range from 0.22 and 0.09. Finally, we calculated relative density fluctuations ϵ measured *in situ* by PSP at a radial distance from the Sun of $35.7 R_\odot$ during the perihelion #1, and the perihelion #2 to be 0.07 and 0.06, respectively. It is in a very good agreement with previous *STEREO* predictions ($\epsilon = 0.06 - 0.07$) obtained by remote measurements of radio sources generated at this radial distance.

Keywords: scattering — Sun: radio radiation — solar wind

1. INTRODUCTION

Type III bursts belong among the strongest radio signals routinely observed by both, space-borne and ground-based observatories (Bastian et al. 1998; Miteva et al. 2017). They are generated by electron beams accelerated at reconnection sites of solar flares traveling outward along open magnetic field lines through the corona and the interplanetary medium (Wild 1950). Along their path electron beams interact with the background plasma producing radio emissions at the electron plasma frequency f_{pe} (the fundamental component), and/or at its first harmonic $2f_{pe}$ (the harmonic component) via the plasma emission mechanism (Ginzburg & Zhelezniakov 1958; Cairns & Robinson 1995; Ergun et al. 1998). Generally, the two components can be distinguished when observed simultaneously, which is rather typical at decametric or shorter wavelengths (Stewart 1974). The fundamental component is usually more intense with 2-3 times higher circular polarization (Dulk & Suzuki 1980). However, it is almost impossible to distinguish the two components in time and frequency, or by polarization for type III bursts at longer wavelengths, which are generated in the interplanetary medium (Reiner et al. 1998; Gopalswamy et al. 2005; Krupar et al. 2015). For rare cases when electron beams are detected *in situ* at the spacecraft, the initial radiation is almost always the fundamental component, while in the late phases it may be one or another (Dulk et al. 1998). Currently, there is no observational evidence to choose between the fundamental and harmonic component for interplanetary type III bursts.

Type III bursts can be simultaneously detected over a broad range of longitudes, even if their sources are located behind the Sun (Bonnin et al. 2008). Their apparent radio sources lie at considerably larger radial distances than predicted by electron density models (Reiner et al. 2009; Martínez Oliveros et al. 2012). Furthermore, apparent type III burst source sizes are so extended that may spread over the entire inner heliosphere (Krupar et al. 2014a). These obscure properties are attributed to scattering of radio waves by electron density inhomogeneities as they propagate from the source region to the observer (Steinberg et al. 1984, 1985; Bastian 1994, 1995; Kontar et al. 2017). The role of refraction and scattering of interplanetary radio emissions can be studied using a geometric optics method and Monte Carlo simulations (Hollweg 1968; Melrose 1980; Thejappa et al. 2007; Thejappa & MacDowall 2008; Kontar et al. 2019).

Recently, Krupar et al. (2018) compared decay times of type III bursts between 125 kHz and 1 MHz observed by the Solar TERrestrial Relations Observatory (*STEREO*) spacecraft with results of Monte Carlo simulations. They suggest that the characteristic exponential decay profile of type III bursts could be solely explained by the scattering of the fundamental component between the source and the observer. Krupar et al. (2018) estimated relative electron density fluctuations $\epsilon = \langle \delta n \rangle / \langle n \rangle$ to be 0.06–0.07 at radial distances from the Sun between 8 and 45 solar radii ($1 R_{\odot} = 695,500$ km), where $\langle n \rangle$ represents an average electron density and $\langle \delta n \rangle$ is an average amplitude of variations of an electron density n from its average value $\langle n \rangle$.

Here, we primarily examine radio measurements obtained by the Parker Solar Probe (PSP) mission with a perihelion down to $9.5 R_{\odot}$ and aphelion near ~ 1 astronomical unit ($1 \text{ au} = 149,598,000$ km; Fox et al. 2016). The PSP/FIELDS instrument provides with comprehensive measurements of coronal plasma and magnetic field, plasma waves and turbulence, and radio signatures of solar transients (Bale et al. 2016; Pulupa et al. 2017). We use data recorded by the Radio Frequency Spectrometer (RFS), which is a two-channel digital receiver and spectrometer in the FIELDS suite. Specifically, we analyze time-frequency profiles of type III bursts between 0.5 MHz and 10 MHz recorded by the RFS/Low Frequency Receiver (LFR; 64 logarithmically spaced frequency channels between 10.5 kHz – 1.7 MHz with a temporal resolution of 7 s) and the RFS/High Frequency Receiver (HFR; 64 logarithmically spaced frequency channels between 1.3 MHz – 19.2 MHz with a temporal resolution of 7 s). Frequencies above 10 MHz have been excluded from this study due to insufficient time resolution of RFS/HFR. On the other hand the frequencies below 0.5 MHz are strongly affected by the quasi-thermal noise (QTN; Meyer-Vernet & Perche 1989) due to considerably larger solar wind density near the Sun when compared to 1 au. For a case study we also use radio data recorded by the *Wind*/WAVES and *STEREO*/WAVES instruments with a temporal resolution of 60 s and 35 s, respectively (Bougeret et al. 1995, 2008). Finally, we investigate solar wind density and bulk velocity retrieved by The PSP/Solar Wind Electrons Alphas and Protons (SWEAP) instrument (Kasper et al. 2016).

In this paper, we present a statistical survey of type III burst decay times that can be used to estimate relative electron density fluctuations ϵ in the solar wind. In

Section 2 we present our analysis of RFS measurements (Section 2.1), its comparison to results of Monte Carlo simulations (Section 2.2), and relative density fluctuations ϵ measured in situ by PSP (Section 2.3). Finally, we discuss and summarize our findings in Section 3.

2. OBSERVATION AND ANALYSIS

2.1. Type III Bursts Measurements

We performed a statistical analysis of 30 type III radio bursts observed by PSP during the perihelion #2 (2019 April 1 – 2019 April 10). During this period radial distances from the Sun ranged from $35.7 R_{\odot}$ to $53.8 R_{\odot}$. We included only intense, simple, and isolated emissions. We show an analysis of a type III burst from 2019 April 3 when PSP was at 68° east from a Sun-Earth line at $36.7 R_{\odot}$ from the Sun as an example from our list of events. Figure 1a displays the power spectral density S from the RFS/HFR and RFS/LFR instruments using the average auto spectral data of the V1–V2 dipole input channel. PSP detected the type III burst with an onset time at about 18:48 UT. The type III burst was also measured by the *Wind*/WAVES and *STEREO-A*/WAVES instruments (Figures 1b and 1c). During this event, the *Wind* spacecraft was on a Sun-Earth line at 0.99 au from the Sun, whereas *STEREO-A* was at 97° east and 0.97 au from the Sun. We have analyzed time delays between peak fluxes for close frequency channels of 609 kHz, 625 kHz, and 624 kHz for PSP, *STEREO-A*, and *Wind*, respectively. We selected these channels as higher frequencies were not observed by *Wind*, while a PSP radio signal at lower frequencies was affected by QTN. The type III burst was delayed by $\delta t_{STA} = 377$ s, and $\delta t_{Wind} = 488$ s between PSP and *STEREO-A* and *Wind*, respectively.

A solar flare triggering this emission has been located on the far side of the Sun from a view of the Earth. Hence we cannot retrieve its intensity and location as spacecraft embarking X-ray imagers orbit the Earth. However, the active region has been observed by *STEREO-A*/Sun Earth Connection Coronal and Heliospheric Investigation/Extreme Ultraviolet Imager (SECHI/EUVI; Howard et al. 2008). We have used the wavelet technique by Stenborg et al. (2008) to produce a composite image for the 171\AA and 195\AA channels (Figure 2). The coordinates for the footpoint of the loops where some activity is observed at 195\AA are $[-131^{\circ}, 6^{\circ}]$ in Stonyhurst-Heliographic longitude and latitude (see the Figure 2 animation).

The favorable configuration of *Wind* and *STEREO-A* allows us to accurately locate the sources of the type III bursts by radio triangulation (Krupar et al. 2014a, 2016). We identified data points that correspond to

peak fluxes for four pairs of frequency channels observed by *Wind*/WAVES (428 kHz, 484 kHz, 548 kHz, and 624 kHz) and *STEREO-A*/WAVES (425 kHz, 475 kHz, 525 kHz, 625 kHz) with signals above background levels. We triangulated the radio sources using wave vector directions during these peak fluxes (Figure 3). Specifically, we consider radio source location to be the closest point between the two wave vectors, and the shortest distance between the wave vectors indicates the error of triangulated source. We also included the Parker spiral rooted in the solar flare site assuming a solar wind speed of 400 km s^{-1} to illustrate a possible path followed by the electron beam (a red dashed line; Parker 1958). Generally, triangulated source regions of higher frequencies are closer to the Sun. Obtained error bars are noticeable only in the XZ_{HEEQ} plane due to the considerable smaller separation angle between *STEREO-A* and *Wind* in this plane (Figure 3d). We have also calculated light travel times between the triangulated radio source at 625/624 kHz and all three spacecraft: $\Delta t_{PSP} = 95$ s, $\Delta t_{STA} = 413$ s, and $\Delta t_{Wind} = 544$ s. Using exclusively radio triangulation, we estimated the radio signal delays between PSP and *STEREO-A* and *Wind* to be $\delta t_{STA} = \Delta t_{STA} - \Delta t_{PSP} = 318$ s and $\delta t_{Wind} = \Delta t_{Wind} - \Delta t_{PSP} = 449$ s, respectively. These values are comparable with actual delay signal measurements shown in Figure 1 ($\Delta t_{STA} = 377$ s, and $\Delta t_{Wind} = 488$ s), which indicates that the radio triangulation technique provides reasonable source locations. Results of the triangulation confirm that the electron beam triggering the type III burst propagates roughly along the Parker spiral field near PSP. The signal measured by *STEREO-A*/WAVES was significantly stronger than that measured by *Wind*/WAVES, which is consistent with the radio source located closer to *STEREO-A*/WAVES. Unfortunately, we are unable to perform the radio propagation analysis using PSP measurements as the PSP effective antenna parameters are not determined yet.

Figure 4 shows fixed frequency light curves of the same event in four frequency channels (0.5 MHz, 1 MHz, 2 MHz, 5 MHz, and 10 MHz). The exponential decay of the power spectral density S over several decades can be identified. For the further analysis, we calculated median values of the power spectral density S frequency by frequency to estimate background level (red lines in Figure 4). We analyze data points between the peak time (t_{peak}) and the last value above this level (*i.e.*, between dashed blue lines in Figure 4). We assume an exponential decay profile of the power spectral density S , that can be described by following equation:

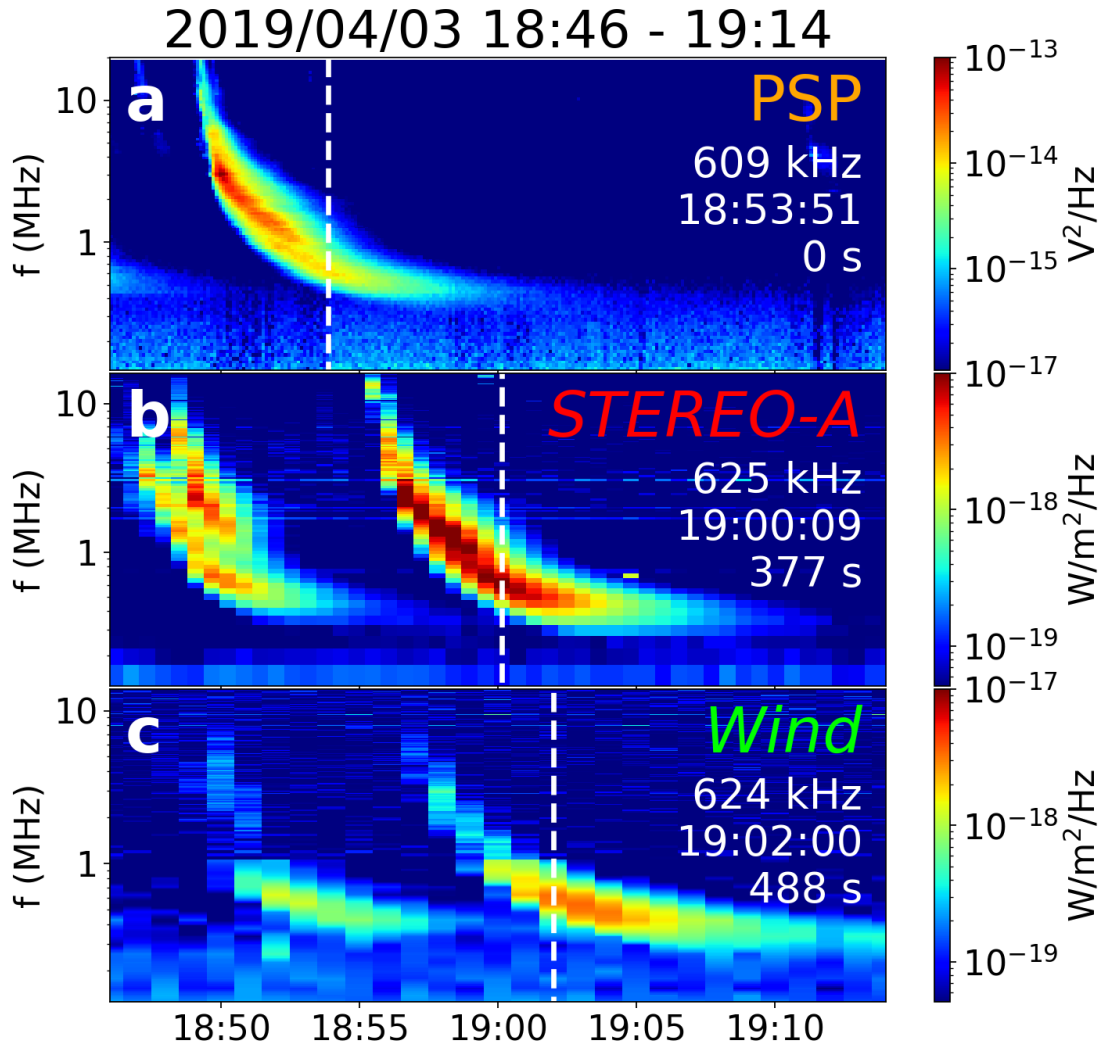


Figure 1. Radio measurements of the 2019 April 3 type III burst. (a) The power spectral density V_r^2 for PSP/RFS. (b) The power flux density S for *STEREO-A*/WAVES. (c) The power flux density S for *Wind*/WAVES. White dashed lines indicate times of peak fluxes at 609 kHz, 625 kHz, and 624 kHz.

$$S(t) = \frac{I}{\tau_d} \exp\left(-\frac{t_{\text{peak}} - t}{\tau_d}\right), \quad (1)$$

where t is the time, t_{peak} corresponds to the time of the peak power spectral density. Coefficients I and τ_d are parameters of a gradient-expansion algorithm used to compute a non-linear least squares fit. Figure 4 shows results of this fitting for decay power spectral density profiles in green.

Figure 5 shows type III burst decay times as a function of frequency for RFS, *STEREO-A*/WAVES, and *Wind*/WAVES. We have achieved a very good agreement between RFS and *STEREO-A*/WAVES for overlapping frequency channels (*i.e.*, between 0.5 MHz and 1 MHz). However, decay times retrieved by *Wind*/WAVES are considerably larger. It can be attributed to different emissions directivity due to rela-

tive spacecraft locations, when PSP and *STEREO-A* are nearly along one Parker spiral, while *Wind* is about 90° away in the solar equatorial plane (Figure 3a). Next, we assume that the decay times τ_d are frequency dependent as:

$$\tau_d(f) = \alpha f^\beta. \quad (2)$$

This model fits the data well for all three spacecraft. We obtained the following spectral indices: $\beta_{\text{PSP}} = (-0.63 \pm 0.02)$, $\beta_{\text{STEREO-A}} = (-1.57 \pm 0.10)$, and $\beta_{\text{Wind}} = (-1.81 \pm 0.22)$. These values were calculated by minimizing the χ^2 error statistic with the $1-\sigma$ uncertainty estimates. Despite variations in decay times between *STEREO-A*/WAVES and *Wind*/WAVES, the obtained spectral indices are rather similar. On the other hand, the β_{PSP} is significantly larger due to contributions by frequency channels between 1 MHz and

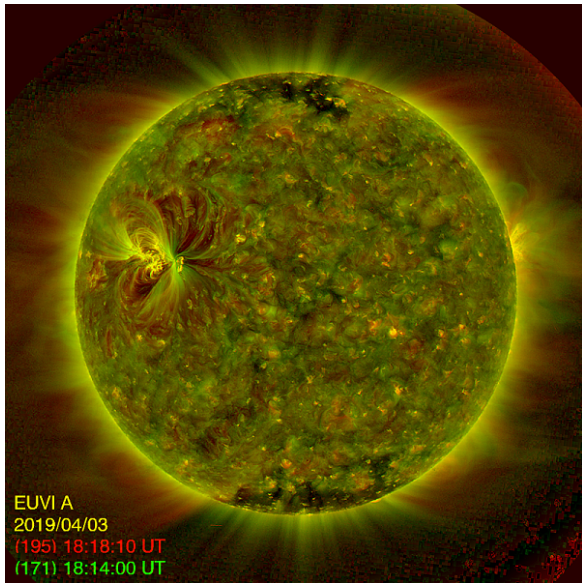


Figure 2. Image of the Sun taken by the *STEREO-A*/SECCHI/EUVI on 2019 April 3 at 18:14:00 UT (171Å) and 18:18:10 UT (195Å). Enhanced images for individual wavelength channels are available at <http://sd-www.jhuapl.edu/secchi/wavelets/fits/201904/03/>. An animation of just the SECCHI/EUVI (195Å) sequence is available. The animation field of view is zoomed in to the area around the flare in the upper right quadrant of the full solar image shown in the figure. The video begins on 2019 April 3 at 18:00:30 and ends the same day at 20:05:30. The realtime duration of the video is 2 seconds. The movie of the solar flare is derotated using the reference time corresponding to the first image (18:00 UT).

10 MHz, which are not covered by *STEREO-A*/WAVES and *Wind*/WAVES.

We performed the above-described analysis of the exponential decay times τ_d on 30 type III bursts observed by PSP during the perihelion #2 case by case. We provide the list of type III burst time-frequency intervals, that can be used for further investigation by the community (Table 1). Figure 6 displays median values of decay times τ_d as a function of frequency. We assume that the decay times τ_d are frequency dependent as a power law (equation 2). The model fits the data very well. We obtained the spectral indices β_{PSP} of -0.60 ± 0.1 .

2.2. Monte Carlo Simulations

Thejappa et al. (2007) developed a Monte Carlo simulation code to investigate a role of refraction and scattering on propagation of interplanetary radio emissions with isotropic sources, when observed by spacecraft at 1 au. For the refraction, the solar wind electron density model of Bougeret et al. (1984) was used ($n \sim r^{-2.10}$). For the scattering, Thejappa et al. (2007) assumed the power spectrum of electron density fluctuations in the

Table 1. The list of type III burst time-frequency intervals

Date begin	Date end	Frequency low	Frequency high
(UTC)	(UTC)	(MHz)	(MHz)
2019-04-01 01:57:00	2019-04-01 02:05:00	1.196	9.572
2019-04-01 17:10:00	2019-04-01 17:17:00	0.545	8.428
2019-04-01 20:25:00	2019-04-01 20:40:00	0.577	7.725
2019-04-02 02:40:00	2019-04-02 02:57:00	0.809	9.572
2019-04-02 04:44:00	2019-04-02 05:00:00	0.514	8.822
2019-04-02 09:01:15	2019-04-02 09:12:00	0.764	9.572
2019-04-03 04:00:00	2019-04-03 04:10:00	1.575	9.572
2019-04-03 06:00:00	2019-04-03 06:10:00	1.566	9.572
2019-04-03 09:20:00	2019-04-03 09:35:00	0.646	9.572
2019-04-03 12:10:00	2019-04-03 12:25:00	0.514	9.572
2019-04-03 12:35:00	2019-04-03 12:50:00	0.514	5.222
2019-04-03 16:48:00	2019-04-03 17:00:00	0.514	9.572
2019-04-03 17:00:00	2019-04-03 17:07:00	1.622	5.972
2019-04-03 18:48:00	2019-04-03 19:00:00	0.514	9.572
2019-04-03 21:05:00	2019-04-03 21:15:00	1.622	9.572
2019-04-03 22:20:00	2019-04-03 22:40:00	0.514	9.572
2019-04-04 02:35:00	2019-04-04 02:50:00	0.646	9.572
2019-04-04 05:33:00	2019-04-04 05:45:00	0.764	9.572
2019-04-04 22:10:00	2019-04-04 22:30:00	0.514	9.572
2019-04-04 22:30:00	2019-04-04 22:40:00	0.646	9.572
2019-04-05 03:25:00	2019-04-05 03:40:00	0.514	9.572
2019-04-05 04:32:00	2019-04-05 04:42:00	0.855	9.572
2019-04-05 10:52:00	2019-04-05 11:00:00	1.481	9.572
2019-04-05 16:52:00	2019-04-05 17:15:00	0.514	9.572
2019-04-05 17:06:00	2019-04-05 17:30:00	0.514	8.072
2019-04-06 07:45:00	2019-04-06 07:59:00	0.514	9.572
2019-04-06 09:40:00	2019-04-06 09:59:00	0.514	9.572
2019-04-06 10:40:00	2019-04-06 10:59:00	0.514	9.572
2019-04-07 09:50:00	2019-04-07 10:00:00	0.957	9.572
2019-04-10 14:25:00	2019-04-10 14:45:00	1.566	9.572

solar wind P_n in the inertial range to be proportional to the Kolmogorov spectrum. The relative electron density fluctuations ϵ was set to be 0.07. We have modified the Monte Carlo technique of Thejappa et al. (2007) to simulate arrival times t_{MC} of radio emissions to $35.7 R_{\odot}$ (*i.e.*, a radial distance of PSP during the perihelion #2). Contrary to Thejappa et al. (2007), we have used a ten times finer simulation grid, variable values of the inner scale l_i (Coles & Harmon 1989), and the Sittler & Guhathakurta (1999) density model, which works better for frequencies above 1 MHz.

Figure 7 shows histograms of simulated arrival times t_{MC} of rays generated at 2 MHz for four levels of the relative electron density fluctuations ($\epsilon = 0.05, 0.10, 0.15, 0.20$). We assumed a presence of the fundamental component only in accordance with Krupar et al. (2018). We identify similar exponential decay profiles as for the RFS measurements in Figure 4. We assume that the number of rays can be directly compared to the power spectral density S . We have applied

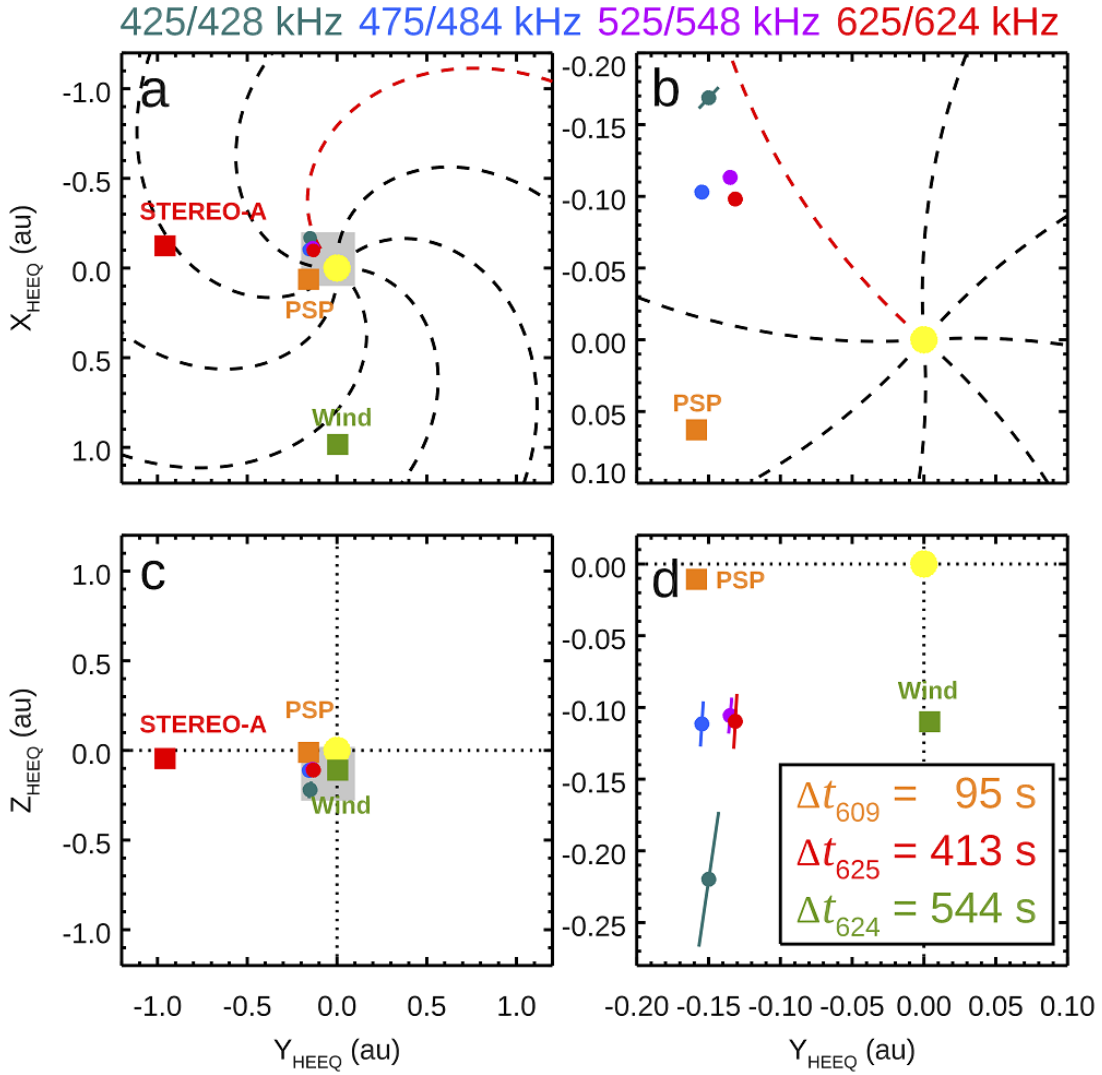


Figure 3. Radio propagation analysis of the 2019 April 3 type III burst. (a)–(d) Triangulated type III burst locations by *STEREO-A* and *Wind* in the XY_{HEEQ} (top) and ZY_{HEEQ} (bottom) planes. Colors denote frequencies shown on the top. Rectangles show spacecraft locations. Dashed lines indicate Parker spirals (a red one is rooted in the solar flare location). Grey areas in panels a and c show axis ranges in panels b and d, respectively.

the same approach as for RFS data to derive the decay times τ_d from these histograms (Figure 4). We have found that the exponential model described by equation 1 is in a good agreement with simulated data. A direct comparison between PSP observations (Figure 4c) and Monte Carlo simulations (Figures 7b and 7c) suggests the relative electron density fluctuations ϵ at the effective turbulence scale length to be between 0.10 and 0.15 for emission generated at 2 MHz.

Next, we performed the Monte Carlo simulations for 5 frequency channels (0.5 MHz, 1 MHz, 2 MHz, 5 MHz, and 10 MHz), and 16 levels of the relative electron density fluctuations ϵ between 0.08 and 0.23. Figure 8a shows simulated and observed decay times τ_d vs. frequency f . While previous analysis of the *STEREO*

data by Krupar et al. (2018) suggested that observed decay times τ_d can be explained by scattering due to nearly constant relative electron density fluctuations ($\epsilon = 0.06 - 0.07$), we need variable values to interpret the PSP data ($\epsilon = 0.09 - 0.22$). Figure 8a displays relative density fluctuations ϵ as a function of frequency. The higher frequencies require larger levels of ϵ to explain observed decay times τ_d by PSP. We have found that this relation can be described by a power law as:

$$\epsilon(f) = \alpha f^\beta. \quad (3)$$

Next, we have converted frequencies to radial distances using the Sittler & Guhathakurta (1999) density model (Figure 9). The obtained relation can be described by power-law type with a spectral index of

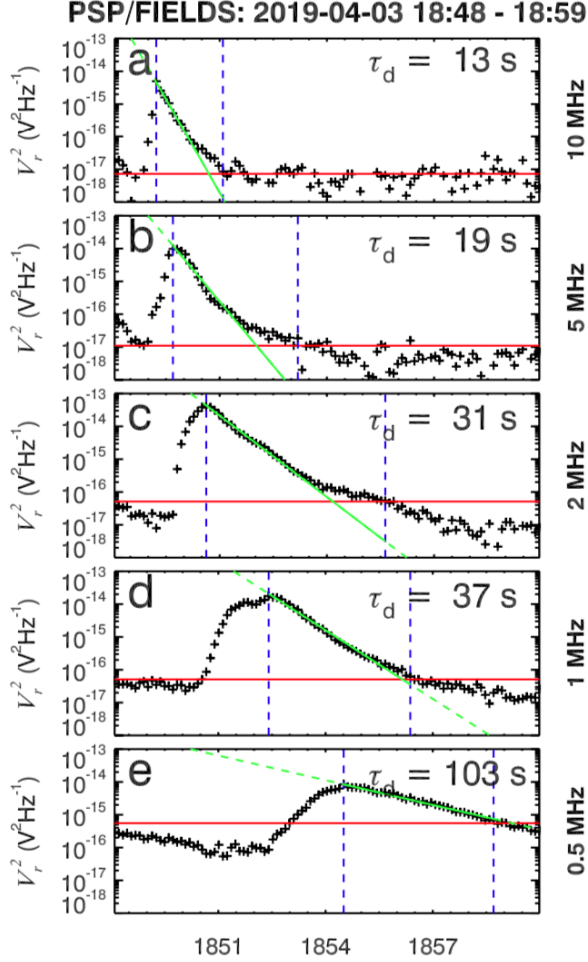


Figure 4. Radio measurements of the 2019 April 3 type III burst. (a)–(e) Fixed frequency light curves of the voltage power spectral density recorded by the RFS instrument for five frequency channels. Red lines show median values in given time intervals. Dashed blue lines denote peak fluxes and last points above median values. Green lines show results of decay time fitting (equation 1).

-0.55 ± 0.01 for radial distances from $2.4 R_{\odot}$ up to $13.9 R_{\odot}$. We note that *STEREO* results between 125 kHz and 1 MHz (*i.e.*, from $8.4 R_{\odot}$ up to $45.1 R_{\odot}$) suggest nearly constant relative density fluctuations $\epsilon = 0.06 - 0.07$ at the effective turbulence scale length (Krupar et al. 2018).

2.3. Density Fluctuations

Finally, we have compared predicted relative density fluctuations by *STEREO* (Krupar et al. 2018), and the measured ones by PSP/SWEAP during the perihelions #1 and #2. Specifically, we use density and velocity measurements based on the proton moments from the SPC Faraday cup. We have calculated median values of plasma density and bulk velocity during periods 12 hours before and 12 hours after the closest approaches

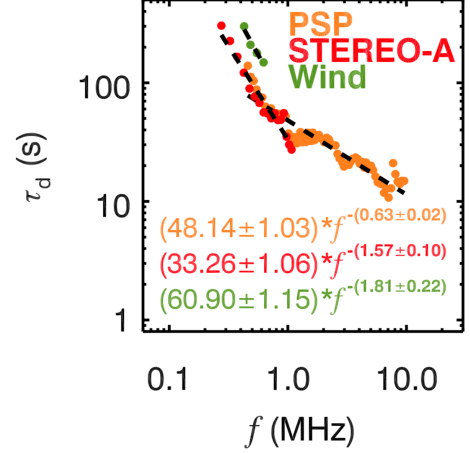


Figure 5. Radio measurements of the 2019 April 3 type III. Decay times τ_d for PSP, *STEREO-A*, and *Wind* as a function of frequency are shown in orange, red, and green, respectively.

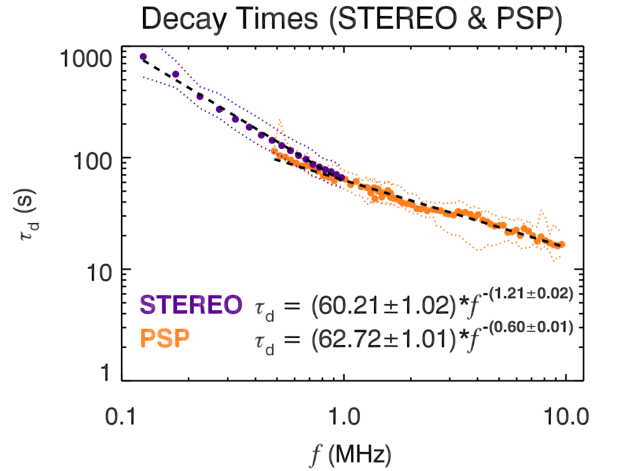


Figure 6. Results of the statistical survey of 152 and 30 type III radio bursts for *STEREO* and PSP. Median values of decay times τ_d for *STEREO* and PSP as a function of frequency are shown in purple and orange, respectively. Error bars are 25th/75th percentiles. Dashed black lines represent results of power-law fitting for the two data sets separately (equation 2).

(Figures 10a–10d). Obtained plasma densities corresponds to local plasma frequencies $f_p = 137$ kHz and $f_p = 86$ kHz for the perihelions #1 and #2, respectively. The Monte Carlo technique assumes the fundamental emission to be generated at $1.05f_p$ resulting in $f = 143$ kHz and $f = 91$ kHz. Next, we retrieve effective spatial scales l_{eff} for these frequencies using empirically derived model of the inner and outer scales of the electron density fluctuations. We compared these spatial scales with median values of plasma bulk velocities to obtain effective temporal scales of the density tur-

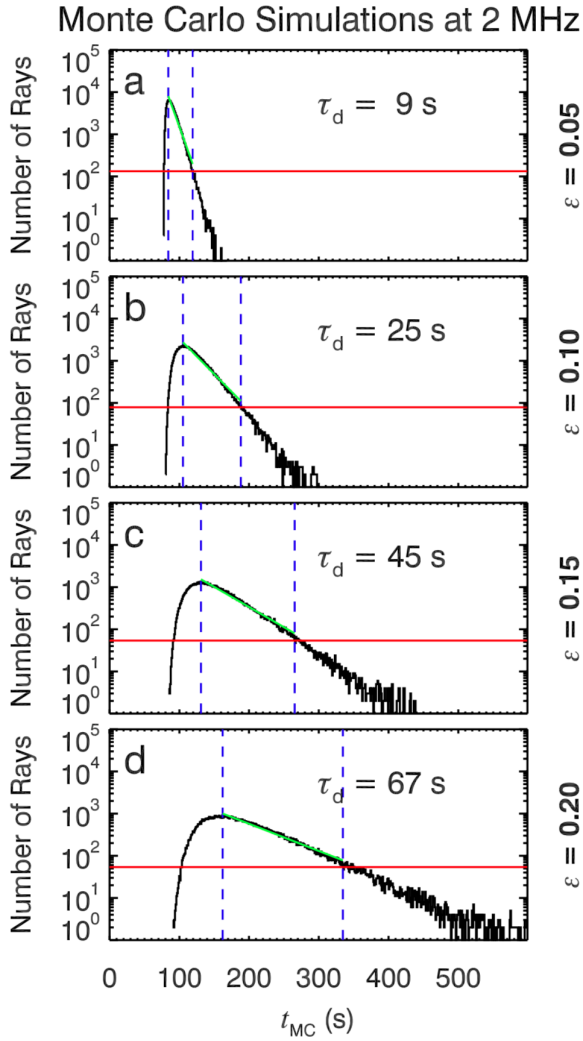


Figure 7. Results of Monte Carlo simulations at 2 MHz. (a)–(d) Histograms of simulated time arrivals t_{MC} for various levels of relative electron density fluctuations ϵ . Red lines show median values. Dashed lines denote peak fluxes and last points above median values. Green lines show results of decay time fitting (Equation 1).

bulence t_{eff} . Next, we have calculated relative density fluctuations ϵ as a function of the time scale t between 10 seconds and 100 minutes:

$$\epsilon(t) = \frac{\langle |n - \langle n \rangle_t| \rangle_t}{\langle n \rangle_t} \quad (4)$$

For time scales corresponding to the effective turbulence scale length in our Monte Carlo simulation technique we obtained $\epsilon = 0.07$ and $\epsilon = 0.06$ for the perihelions #1 and #2, respectively. It is in a very good agreement with relative density fluctuations $\epsilon = 0.06 - 0.07$ predicted by Krupar et al. (2018).

3. DISCUSSION AND SUMMARY

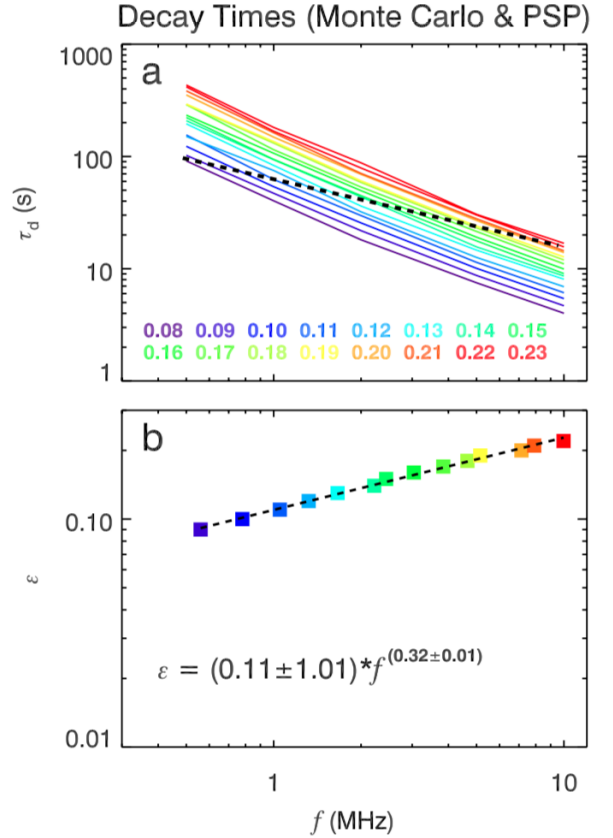


Figure 8. Comparison of Monte Carlo simulations and PSP observations. (a) Simulated decay times τ_d as a function of frequency for 16 levels of relative density fluctuations ϵ in color. A dashed black line shows fitting results from PSP (Figure 6). (b) Relative density fluctuations ϵ as a function of frequency retrieved from intersections between Monte Carlo simulations and PSP observations. A dashed black line represents results of power-law fitting.

While type III bursts have been observed for almost 70 years, a proper model to explain their obscure properties is still missing. PSP/RFS is the state-of-the-art instrument which allows us to investigate interplanetary solar radio bursts with an unprecedented time resolution near the Sun. For the first time, we can accurately retrieve type III burst decay times for frequencies between 1 MHz and 10 MHz to remotely probe solar wind turbulence near the Sun. Although PSP/RFS accumulated wealth of data during the first two perihelions, type III bursts were almost exclusively observed during the perihelion #2 only despite the ongoing solar minimum.

We show an analysis of a type III burst that occurred on 2019 April 3 during the perihelion #2 (Figure 1), which was associated with the active region at $[-131^\circ, 6^\circ]$ in Stonyhurst-Heliographic longitude and latitude (Figure 2). We note that this active region was

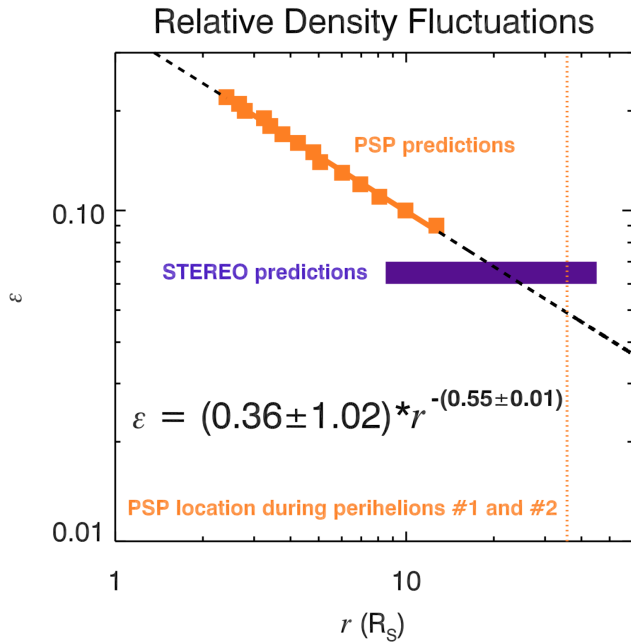


Figure 9. Results of Monte Carlo simulations and PSP observations. Relative density fluctuations ϵ from Figure 8b as a function of radial distance r are denoted by orange squares. A solid black line represent results of power-law fitting. Predicted relative density fluctuations ϵ by *STEREO* are shown in purple. A dotted orange line indicates radial distance of PSP during the Perihelion #1 and #2.

responsible for a majority of solar activity during the perihelion #2. The simple type III burst was also observed couple minutes later by *STEREO-A* and *Wind*, which allowed us to compare signal delays between the three spacecraft. We have localized radio sources using triangulation technique applied to *STEREO-A/Waves* and *Wind/Waves* measurements (Figure 3). Triangulated radio sources lie near the modeled Parker spiral rooted in the active region. The results from the radio triangulation and time delay analysis confirm that this radio emission is related to the active region.

We have analyzed RFS fixed frequency light curves for five frequency channels (Figure 4; 0.5 MHz, 1 MHz, 2 MHz, 5 MHz, and 10 MHz). We observed the characteristic exponential decay profile for all frequency channels. However, the fit does not perform well for late phases at higher frequencies and a clear hardening of the profile can be recognized. This effect is probably related to underestimating of background level for the exponential decay fit at higher frequencies. While the type III burst is above the estimated background level for almost six minutes at 0.5 MHz, it is only around two minutes at 10 MHz. Consequently, the background level at 10 MHz on the same 11 minute time interval is relatively lower when compared to measurements at

0.5 MHz. Other explanation would be a presence of the harmonic component and/or another weaker type III burst. Nevertheless, these deviations in late phases are of minor importance to affect calculated decay times since obtained values predominantly rely on data points succeeding peak fluxes, where the exponential decay fit performs very well.

Figure 5 shows a comparison of decay times observed by all three spacecraft. Despite different radial distances of PSP and *STEREO-A* from the Sun, obtained results are comparable for overlapping frequencies as the two spacecraft lie approximately on the same Parker spiral. It indicates that scattering – if responsible for long exponential decays – occurs primarily near sources, and radio waves propagate along straight lines afterwards. Nonetheless, the exponential decay exhibits a clear hardening above 1 MHz, which will be discussed later. We note that the hardening would be even more pronounced if the late phases in Figure 4 are included.

On the other hand, decay times observed by *Wind* are considerably longer perhaps due to larger longitudinal separation with the active region. However, the slope of the power-law fit is similar to *STEREO-A*. A comparison of decay times from widely separated spacecraft may provide additional information to radio triangulation and/or time delay analysis to complement radio source localization.

We have investigated a large number of type III bursts in order to statistically retrieve their exponential decay times τ_d as a function of frequency f (Figure 6). Using the power-law model we obtain a spectral index β_{PSP} of -0.60 ± 0.01 . Recently, Krupar et al. (2018) performed a similar analysis of 152 type III bursts between 125 kHz and 1 MHz observed by the *STEREO* spacecraft located at 1 au. The obtained spectral index is about twice smaller than for PSP ($\beta_{\text{STEREO}} = -1.21 \pm 0.01$). However, statistical results between 0.5 MHz and 1 MHz by both PSP (30 events detected in April 2019 at ~ 0.17 au) and *STEREO* (152 events measured between May 2007 and February 2013 at ~ 1 au) are comparable. If one assumes that exponential decay is caused by scattering, then it confirms that scattering is important only close to radio sources and later type III bursts propagate along straight lines.

The Sittler & Guhathakurta (1999) density model suggests that 1 MHz – where the slope changes between *STEREO* and PSP – corresponds to a radial distance of $\sim 8 R_{\odot}$ (the fundamental component) or $\sim 14 R_{\odot}$ (the harmonic component), where the solar wind speed typically exceeds the Alfvén speed, and the solar wind become superalfvénic – the solar wind is no longer in contact with the Sun since Alfvén waves can-

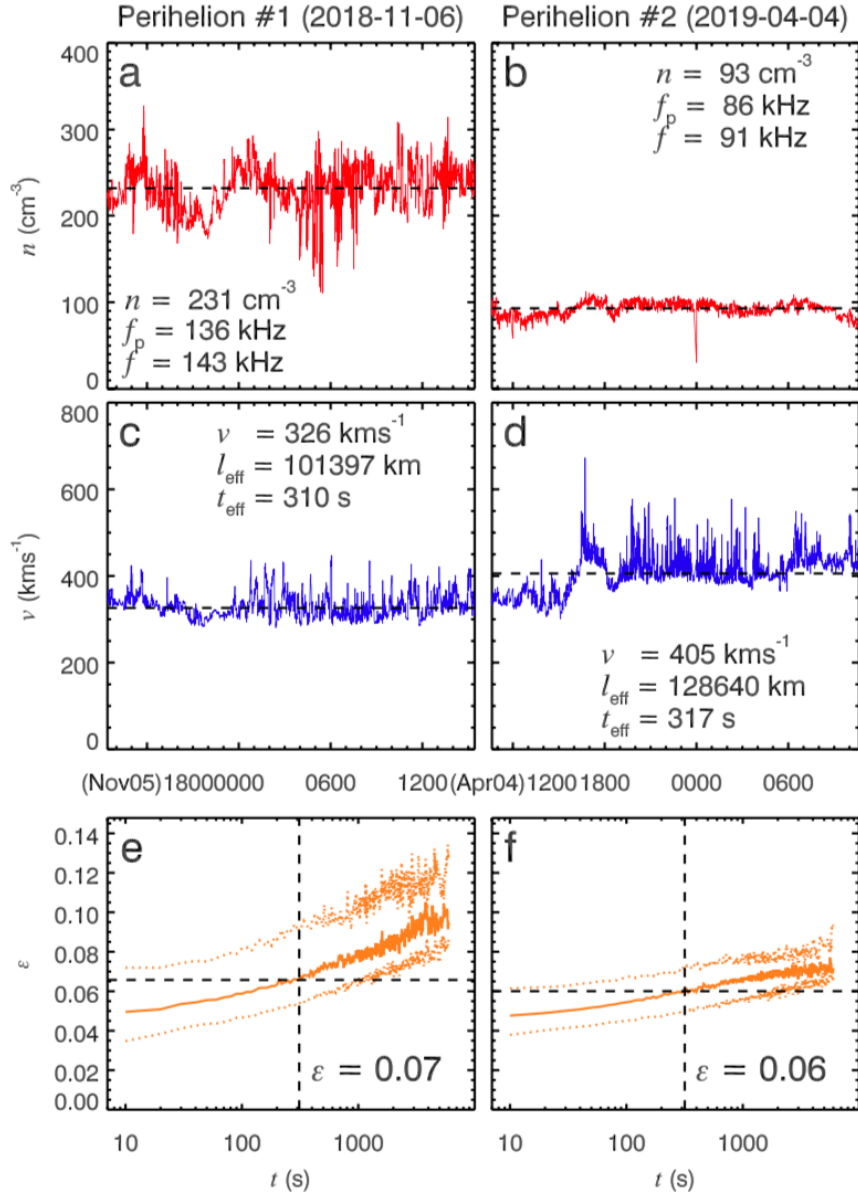


Figure 10. PSP plasma measurements 12 hours before and 12 hours after the perihelion #1 (left) and perihelion #2 (right). (a,b) Plasma density. (c,d) Bulk velocity. Dashed black lines show median values. (e,f) Median values of relative density fluctuations ϵ as a function of temporal scale t . Error bars are 25th/75th percentiles. Dashed black lines correspond to the effective scales of Monte Carlo simulations for frequency of 143 kHz and 91 kHz obtained from plasma parameters obtained during the perihelion #1 and perihelion #2.

not travel back to the Sun Type III burst properties change around 1 MHz as the ambient plasma evolves significantly. Moreover, type III bursts statistically exhibit also a maximum of power spectral density around 1 MHz (Krupar et al. 2014b). Furthermore, it is also possible that we rather observe the fundamental component below 1 MHz, while the harmonic component is dominant above 1 MHz. If it is the case, variations in exponential decay times within one single type III burst can be used to distinguish the component one from another.

We have implemented a Monte Carlo simulation technique to study a role of scattering to type III burst decay times (Figure 7). We assumed a presence of the fundamental component only since the used Monte Carlo simulation technique does not perform well for the harmonic one. Specifically, Krupar et al. (2018) showed that distributions of simulated arrival times of the harmonic component are very narrow with short onset times, which is inconsistent with type III burst observations. Moreover, following assumptions have been included in the Monte Carlo code: (1) an isotropic point

source, (2) the Sittler & Guhathakurta (1999) density model, (3) a power-law distribution of density fluctuations, (4) empirically modeled inner and outer scales, (5) a constant value of isotropic density fluctuations. Obviously, these simplifications affect our analysis and can be improved in the future. For example, a finite size dipole/quadrupole emission pattern would probably slightly increase modeled decay times. A variable anisotropic density fluctuation model would work better for radio emission generated near the Sun.

From the arrival times we calculated the decay times τ_d that we compare to those observed by RFS (Figure 8). As scattering plays a significant role near radio sources only, we may assume variable levels of ϵ when comparing PSP observations with Monte Carlo simulations for each frequency separately. Our results suggest that the exponential decay of the observed power spectral density can be explained by the scattering of radio signal by density inhomogeneities in the solar wind. Obtained relative electron density fluctuations ϵ are 0.09 – 0.22 at the effective turbulence scale length. We note that this range depends on our assumptions of the effective scale l_{eff} of the electron density fluctuations near actual radio sources.

Predicted electron density fluctuations increase closer to the Sun below the Alfvén point (Figure 9). Nonetheless, *STEREO* observations indicate constant density fluctuations above the Alfvén point (Krupar et al. 2018). Possible explanation of this discrepancy would be that solar wind turbulence is primarily formed near the Sun, while it remains frozen into the solar wind once beyond the Alfvén point.

Finally, we have analyzed plasma parameters measured *in situ* by PSP during the perihelion #1 and the perihelion #2 to exploit unique observations near the Sun (Figure 10). Our results suggest that relative density fluctuations ϵ are 0.06 – 0.07 at the effective turbulence scale length in our Monte Carlo simulation technique, which confirm previous predictions by Krupar et al. (2018).

The main results of this study have been obtained by a statistical analysis of 30 type III bursts observed by PSP during the perihelion #2, by Monte Carlo modeling of radio wave propagation in the solar wind, and by an analysis of *in situ* plasma measurements during the perihelion #1, and the perihelion #2. We have concluded that:

1. Type III burst decay times between 0.5 MHz and 1 MHz are statistically comparable at ~ 0.17 au and ~ 1 au, which confirms that scattering plays a major role in radio wave propagation near sources only.
2. Type III burst decay times between 1 MHz and 10 MHz are statistically longer than expected based on previous observations at lower frequencies. It can be explained either by different ambient plasma parameters above the Alfvén point or that we observe preferably the harmonic component above 1 MHz.
3. If the latter is true, variations in exponential decay times can be used to distinguish fundamental and harmonic components within one single type III burst.
4. By comparing PSP observations and Monte Carlo simulations, we predicted relative density fluctuations ϵ at radial distances between $2.5 R_{\odot}$ and $14 R_{\odot}$ to range from 0.22 and 0.09.
5. Observed relative density fluctuations ϵ at a radial distance from the Sun of $35.7 R_{\odot}$ were 0.06 – 0.07.

Note, however, that predicted relative density fluctuations ϵ are based on an assumption that we primarily observe the fundamental component of type III bursts only as the used Monte Carlo technique does not perform well for the harmonic component (Krupar et al. 2018).

ACKNOWLEDGMENTS

The authors would like to thank the many individuals and institutions who contributed to making PSP, *STEREO*, and *Wind* possible. V.K. acknowledges support by an appointment to the NASA postdoctoral program at the NASA Goddard Space Flight Center administered by Universities Space Research Association under contract with NASA and the Czech Science Foundation grant 17-06818Y. O.K. thanks support of the Czech Science Foundation grant 17-06065S. E.P.K. was supported by an STFC consolidated grant ST/P000533/1. S.D.B. acknowledges the support of the Leverhulme Trust Visiting Professorship program. Data access and processing was performed using SPEDAS (Angelopoulos et al. 2019). All data is publicly available at <https://spdf.gsfc.nasa.gov/> and <https://umbra.nascom.nasa.gov/>.

REFERENCES

- Angelopoulos, V., Cruce, P., Drozdov, A., et al. 2019, *Space Sci. Rev.*, 215, 9, doi: [10.1007/s11214-018-0576-4](https://doi.org/10.1007/s11214-018-0576-4)
- Bale, S. D., Goetz, K., Harvey, P. R., et al. 2016, *SSRv*, 204, 49, doi: [10.1007/s11214-016-0244-5](https://doi.org/10.1007/s11214-016-0244-5)
- Bastian, T. S. 1994, *ApJ*, 426, 774, doi: [10.1086/174114](https://doi.org/10.1086/174114)
- . 1995, *ApJ*, 439, 494, doi: [10.1086/175190](https://doi.org/10.1086/175190)
- Bastian, T. S., Benz, A. O., & Gary, D. E. 1998, *ARA&A*, 36, 131, doi: [10.1146/annurev.astro.36.1.131](https://doi.org/10.1146/annurev.astro.36.1.131)
- Bonnin, X., Hoang, S., & Maksimovic, M. 2008, *Astronomy and Astrophysics*, 489, 419, doi: [10.1051/0004-6361/200809777](https://doi.org/10.1051/0004-6361/200809777)
- Bougeret, J.-L., King, J. H., & Schwenn, R. 1984, *Solar Physics*, 90, 401, doi: [10.1007/BF00173965](https://doi.org/10.1007/BF00173965)
- Bougeret, J.-L., Kaiser, M. L., Kellogg, P. J., et al. 1995, *Space Science Reviews*, 71, 231, doi: [10.1007/BF00751331](https://doi.org/10.1007/BF00751331)
- Bougeret, J. L., Goetz, K., Kaiser, M. L., et al. 2008, *Space Sci. Rev.*, 136, 487, doi: [10.1007/s11214-007-9298-8](https://doi.org/10.1007/s11214-007-9298-8)
- Cairns, I. H., & Robinson, P. A. 1995, "Astrophysical Journal", 453, 959, doi: [10.1086/176456](https://doi.org/10.1086/176456)
- Coles, W. A., & Harmon, J. K. 1989, *ApJ*, 337, 1023, doi: [10.1086/167173](https://doi.org/10.1086/167173)
- Dulk, G. A., Leblanc, Y., Robinson, P. A., Bougeret, J.-L., & Lin, R. P. 1998, *J. Geophys. Res.*, 103, 17223, doi: [10.1029/97JA03061](https://doi.org/10.1029/97JA03061)
- Dulk, G. A., & Suzuki, S. 1980, *Astronomy and Astrophysics*, 88, 203
- Ergun, R. E., Larson, D., Lin, R. P., et al. 1998, *ApJ*, 503, 435, doi: [10.1086/305954](https://doi.org/10.1086/305954)
- Fox, N. J., Velli, M. C., Bale, S. D., et al. 2016, *SSRv*, 204, 7, doi: [10.1007/s11214-015-0211-6](https://doi.org/10.1007/s11214-015-0211-6)
- Ginzburg, V. L., & Zhelezniakov, V. V. 1958, *Sov. Astron.*, 2, 653
- Gopalswamy, N., Aguilar-Rodriguez, E., Yashiro, S., et al. 2005, *Journal of Geophysical Research (Space Physics)*, 110, 12, doi: [10.1029/2005JA011158](https://doi.org/10.1029/2005JA011158)
- Hollweg, J. V. 1968, *AJ*, 73, 972, doi: [10.1086/110756](https://doi.org/10.1086/110756)
- Howard, R. A., Moses, J. D., Vourlidas, A., et al. 2008, *Space Sci. Rev.*, 136, 67, doi: [10.1007/s11214-008-9341-4](https://doi.org/10.1007/s11214-008-9341-4)
- Kasper, J. C., Abiad, R., Austin, G., et al. 2016, *SSRv*, 204, 131, doi: [10.1007/s11214-015-0206-3](https://doi.org/10.1007/s11214-015-0206-3)
- Kontar, E. P., Yu, S., Kuznetsov, A. A., et al. 2017, *Nature Communications*, 8, 1515, doi: [10.1038/s41467-017-01307-8](https://doi.org/10.1038/s41467-017-01307-8)
- Kontar, E. P., Chen, X., Chrysaphi, N., et al. 2019, *ApJ*, 884, 122, doi: [10.3847/1538-4357/ab40bb](https://doi.org/10.3847/1538-4357/ab40bb)
- Krupar, V., Kontar, E. P., Soucek, J., et al. 2015, *A&A*, 580, A137, doi: [10.1051/0004-6361/201425308](https://doi.org/10.1051/0004-6361/201425308)
- Krupar, V., Maksimovic, M., Santolik, O., Cecconi, B., & Kruparova, O. 2014a, *Solar Phys.*, 289, 4633, doi: [10.1007/s11207-014-0601-z](https://doi.org/10.1007/s11207-014-0601-z)
- Krupar, V., Maksimovic, M., Santolik, O., et al. 2014b, *Solar Phys.*, 289, 3121, doi: [10.1007/s11207-014-0522-x](https://doi.org/10.1007/s11207-014-0522-x)
- Krupar, V., Eastwood, J. P., Kruparova, O., et al. 2016, *ApJL*, 823, L5, doi: [10.3847/2041-8205/823/1/L5](https://doi.org/10.3847/2041-8205/823/1/L5)
- Krupar, V., Maksimovic, M., Kontar, E. P., et al. 2018, *Astrophys. J.*, 857, 82, doi: [10.3847/1538-4357/aab60f](https://doi.org/10.3847/1538-4357/aab60f)
- Martínez Oliveros, J. C., Lindsey, C., Bale, S. D., & Krucker, S. 2012, *Solar Phys.*, 279, 153, doi: [10.1007/s11207-012-9998-4](https://doi.org/10.1007/s11207-012-9998-4)
- Melrose, D. B. 1980, *Space Science Reviews*, 26, 3, doi: [10.1007/BF00212597](https://doi.org/10.1007/BF00212597)
- Meyer-Vernet, N., & Perche, C. 1989, *Journal of Geophysical Research*, 94, 2405, doi: [10.1029/JA094iA03p02405](https://doi.org/10.1029/JA094iA03p02405)
- Miteva, R., Samwel, S. W., & Krupar, V. 2017, *Journal of Space Weather and Space Climate*, 7, A37, doi: [10.1051/swsc/2017035](https://doi.org/10.1051/swsc/2017035)
- Parker, E. N. 1958, *Astrophysical Journal*, 128, 677, doi: [10.1086/146580](https://doi.org/10.1086/146580)
- Pulupa, M., Bale, S. D., Bonnell, J. W., et al. 2017, *Journal of Geophysical Research (Space Physics)*, 122, 2836, doi: [10.1002/2016JA023345](https://doi.org/10.1002/2016JA023345)
- Reiner, M. J., Kaiser, M. L., Fainberg, J., & Stone, R. G. 1998, *Journal of Geophysical Research*, 103, 29651, doi: [10.1029/98JA02614](https://doi.org/10.1029/98JA02614)
- Reiner, M. J., Goetz, K., Fainberg, J., et al. 2009, *SoPh*, 259, 255, doi: [10.1007/s11207-009-9404-z](https://doi.org/10.1007/s11207-009-9404-z)
- Sittler, Jr., E. C., & Guhathakurta, M. 1999, *Astrophys. J.*, 523, 812, doi: [10.1086/307742](https://doi.org/10.1086/307742)
- Steinberg, J. L., Hoang, S., & Dulk, G. A. 1985, *Astron. Astrophys.*, 150, 205
- Steinberg, J. L., Hoang, S., Lecacheux, A., Aubier, M. G., & Dulk, G. A. 1984, *Astron. Astrophys.*, 140, 39
- Stenborg, G., Vourlidas, A., & Howard, R. A. 2008, *ApJ*, 674, 1201, doi: [10.1086/525556](https://doi.org/10.1086/525556)
- Stewart, R. T. 1974, *SoPh*, 39, 451, doi: [10.1007/BF00162437](https://doi.org/10.1007/BF00162437)
- Thejappa, G., & MacDowall, R. J. 2008, *ApJ*, 676, 1338, doi: [10.1086/528835](https://doi.org/10.1086/528835)
- Thejappa, G., MacDowall, R. J., & Kaiser, M. L. 2007, *Astrophys. J.*, 671, 894, doi: [10.1086/522664](https://doi.org/10.1086/522664)
- Wild, J. P. 1950, *Austr. J. Sci. Res. A Phys. Sci.*, 3, 541